Article

Assessment of Rainstorm Waterlogging Disaster Risk in Rapidly Urbanizing Areas Based on Land Use Scenario Simulation: A Case Study of Jiangqiao Town in Shanghai, China

Hui Xu [1,2,*], Junlong Gao [1], Xinchun Yu [1,*], Qianqian Qin [3], Shiqiang Du [1] and Jiahong Wen [1,2]

[1] School of Environmental and Geographical Sciences, Shanghai Normal University, Shanghai 200234, China
[2] Key Laboratory of Resilient Cities and Integrated Risk Management, Shanghai Emergency Management Bureau, Shanghai 200003, China
[3] Planning School of Architecture Planning and Landscape, Newcastle University, Newcastle upon Tyne NE1 7RU, UK
[*] Correspondence: xuhui@shnu.edu.cn (H.X.); yxchappy0602@163.com (X.Y.)

Abstract: The impact of flooding on cities is becoming increasingly significant in the context of climate change and rapid urbanization. Based on the analysis of the land use changes and rainstorm waterlogging inundation scenarios of Jiangqiao Town from 1980 to 2020, a scenario analysis was conducted to simulate and assess the rainstorm waterlogging disaster risk in 2040 under three land use scenarios (a natural development scenario, Scenario ND; an economic growth scenario, Scenario EG; and an ecological development priority scenario, Scenario EP) and three rainstorm scenarios with return periods of 10, 50, and 100 years. The following results were found: (1) Land use change is a significant factor in the risk of urban rainstorm waterlogging disaster caused by surface runoff and inundation depth change. In particular, the resultant increase in impermeable surfaces such as residential land and industrial land and the decrease in farmland during urbanization would lead to an increase in urban rainstorm waterlogging disaster risk. (2) Under three rainstorm scenarios, the future land use exposure elements and losses are consistent in terms of spatial distribution; from 10-year to 100-year return periods, they manifest as an expansion from the south to the surroundings, especially to the central region of the study area. The locations at risk are mainly distributed in the central and southern regions of Jiangqiao Town. (3) The economic losses are different in different land use scenarios and rainstorm scenarios. In the context of rainstorm scenarios with return periods of 10, 50, and 100 years, the total losses in land use scenario ND are CNY 560 million, CNY 890 million, and CNY 1.07 billion; those in land use scenario EG are CNY 630 million, CNY 980 million, and CNY 1.19 billion; and those in land use scenario EP are CNY 480 million, CNY 750 million, and CNY 910 million. The total losses of land use EP are the lowest by comparison. So, the influence of land use change on the rainstorm waterlogging disaster risk shows obvious differences among different rainstorm scenarios. This study has important reference value for decision making on land use management and flood disaster risk management in rapidly urbanizing areas.

Keywords: rainstorm waterlogging disaster risk; risk assessment; land use change; scenario analysis; Shanghai

1. Introduction

Influenced by global climate warming and rapid urbanization, the intensity, frequency, and extent of flood disasters continue to increase. Consequently, urban areas are at an elevated risk of flood disasters [1,2]. According to the Emergency Events Database (EM-DAT), between 2002 and 2021, floods constituted approximately 45% of all disasters annually. The economic losses attributed to floods accounted for, on average, around 22% of the total economic losses caused by all disasters each year. Furthermore, the frequency of flood events exhibited a fluctuating but generally upward trend during this period [3]. Existing

research indicates that rapid urbanization and the resulting significant changes in land use have a significant impact on hydrological processes such as water evapotranspiration, underwater infiltration, and surface runoff [4–8], which increase the risk of rainstorm waterlogging disasters in urban areas [9,10]. In addition, the risk of urban flooding disasters is expected to continue increasing in the context of intensified future climate change and ongoing urbanization [11,12]. Therefore, urban rainstorm waterlogging disasters, as high-probability disaster risk events within flooding disaster scenarios, have emerged as a frontier topic in urban natural disaster risk management research [13–15]. Currently, the risk assessment of urban rainstorm waterlogging disasters primarily focuses on hazards, exposure, and vulnerability [16,17]. Hazard research can be summarized into three aspects: simulation analysis based on probability distribution theory [18,19], inundation simulation analysis based on runoff modeling [20–22], and hazard evaluation based on remote sensing monitoring [23,24]. Research on exposure mainly focuses on elements exposed to risk, including populations [25], buildings [26], agriculture [27], etc. Vulnerability research primarily involves establishing damage curves of exposed elements through methods such as questionnaire surveys or experimental simulations [28–30] to further analyze the potential losses caused by hazards. The above studies have formed a relatively integrated framework for disaster risk assessment.

The research conducted on the mechanisms of land use and flood disaster risk has yielded relatively rich achievements. Previous studies have mostly focused on disaster loss assessment through the simulation of different rainstorm waterlogging scenarios [31,32]. However, research on urban rainstorm waterlogging disaster risk combined with multiple land use scenarios with multiple rainstorm scenarios is relatively scarce [33,34]. Some studies have highlighted that land use changes could mitigate or exacerbate urban rainstorm waterlogging disaster risk [35] to some extent by affecting precipitation runoff [36,37]. Therefore, research related to reducing flood disaster risk by optimizing land use has been brought to the forefront. In recent years, nature-based solutions (NbS) to land use optimization, coping with climate change, and disaster risk reduction have become a new research hotspot [38].

Shanghai is located in the eastern coastal region of China, where floods occur from time to time and have become increasingly frequent in recent years. Coupled with the high population density, extensive infrastructure, and buildings in the region, the impact of flooding is prominent [39–41]. Recently, some scholars have researched urban rainstorm waterlogging disaster risk assessment using Shanghai as a case study [42–45]. However, there has been less focus on risk assessment based on different land use scenarios. Given this, this study focused on Jiangqiao Town in Shanghai, characterized by significant land use changes. By constructing three future land use scenarios, namely, Scenario ND, Scenario EG, and Scenario EP, this study aims to analyze the rainstorm waterlogging disaster risk under multiple rainstorm events and different land use scenarios precipitated by climate change and urbanization. This research provides decision-making references and valuable insights into ways to reduce the impact of urban rainstorm waterlogging disaster risk and enhance urban disaster risk resilience by changing land use patterns.

2. Data and Methods

2.1. Study Area

Jiangqiao Town is located at the intersection of Jiading District, Putuo District, and Minhang District in Shanghai (Figure 1a), with an area of about 42.47 km^2 and a population of about 276,000. It is currently a rapidly urbanizing area of Shanghai that offers convenient transportation. According to the *Jiangqiao Town Master Plan and Land Use Master Plan (2015–2040)*, the urbanization ratio of Jiangqiao Town is 99%. In addition, the overall terrain of Jiangqiao Town is high in the north and low in the south, with elevations ranging from 0 to 2.87 m (Figure 1b), and its soil types can be classified into three categories (Figure 1c). According to Shanghai local chronicles like *The Chronicle of Jiangqiao Township (1949 to 2020)* and the *Jiading District Statistical Yearbook (1988 to 2020)*, news reports, etc., Jiangqiao Town

has experienced at least 30 rainstorms and waterlogging disasters since 1949, especially extreme events like Typhoon Fite in 2013. which had a significant impact on the town.
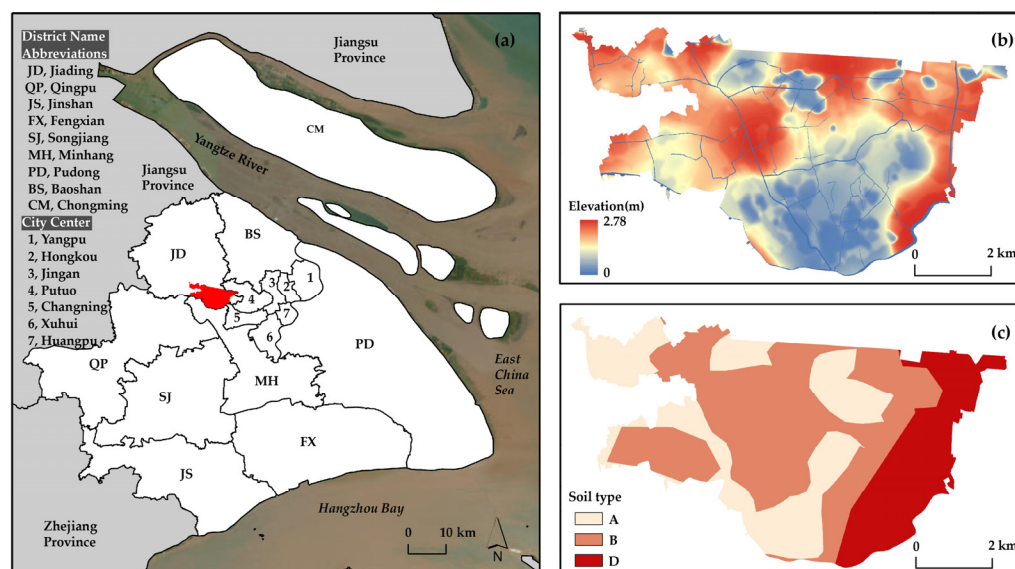

Figure 1. (**a**) Location of Jiangqiao Town in Shanghai. (**b**) Digital elevation model (DEM) of Jiangqiao Town. (**c**) Soil types of Jiangqiao Town.

2.2. Data

Research data used in this article encompass six categories: land use data, elevation data, soil data, precipitation data, depth–damage functions, and economic data related to loss assessment.

Land use data were obtained by interpreting six remote sensing images from 1980, 1990, 2000, 2006, 2013, and 2020. The remote sensing images from 1980 and 1990 were derived from the Geographical Information Monitoring Cloud Platform (http://www.dsac.cn/) (accessed on 27 July 2023), and the remote sensing images from 2000, 2006, 2013, and 2020 were derived from Google Earth. In this study, land use types are classified as transportation land (TL), public building land (PBL), farmland, green land (GL), residential land (RL), industrial land (IL), water area (WA), and other land (OL), where PBL refers to government agencies, healthcare, education, cultural tourism, etc., while IL mainly includes factories, production workshops, handicraft workshops, etc. The overall accuracy of land use for six phases exceeded 0.75. The spatial resolution of the land use data is 10 m by 10 m.

Elevation data were obtained by our group based on a 1:10,000 topographic map (2010) and Lidar data (2010) provided by *Shanghai Surveying and Mapping Institute* [46], with a spatial resolution of 10 m by 10 m.

Soil data were derived from the *Shanghai Soil* database compiled by the *Shanghai Soil Census Office* and the 1:1,000,000 soil map of China published by the *Institute of Soil Science, Chinese Academy of Sciences* (http://www.issas.ac.cn/) (accessed on 10 August 2023). Soil types in Jiangqiao Town mainly include tidal sandy mud, ditch-dry tidal mud, vegetable garden grey tidal mud, ditch-dry mud, loess, and hard pavement. In this study, the Soil Conservation Service (SCS) model was used for surface runoff simulation. According to the SCS model, the soil types of Jiangqiao Town can be classified into three distinct categories (labeled as A, B, and D), where A includes thick sand layers, sandy loam, and so on; B includes thin loess layers, silty loam, and so on; and D includes sandy clay, hard pavement, and so on (Figure 1c). The spatial resolution of soil data is 10 m by 10 m.

Precipitation data were calculated using the Standard of Rainstorm Intensity Formula and Design Rainstorm Distribution (DB31/T 1043–2017) [47] published by Shanghai Engineering Design Institute:

$$q = \frac{1995.84(p^{0.3} - 0.42)}{(t + 10 + 7\ lg\ p)^{0.82 + 0.07\ lg\ p}} \tag{1}$$

where q is the rainstorm intensity (mm/h), t is the precipitation duration (min), and p is the stormwater return period (year). In this study, 1 h precipitation durations corresponding to 10-, 50-, and 100-year return periods are employed. These scenarios correspond to 1 h precipitation amounts of 65.8 mm, 89.7 mm, and 101 mm, respectively.

Depth–damage functions are used to explore the relationship between the damage ratio $f(x)$ (%) and inundation depth x (m). The depth–damage functions of buildings are based on the research conducted by Ke in 2014 [48], the depth–damage functions of indoor properties are based on the research conducted by Quan in 2014 [49], and the depth–damage function of farmland is based on the research conducted by Yin et al. in 2011 [50].

The depth–damage function of buildings on IL and PBL is

$$f(x) = \left(-0.004762x^2 + 0.0919x - 0.01286\right) \times 100\% \tag{2}$$

The depth–damage function of buildings on RL is

$$f(x) = \left(-0.0009524x^2 + 0.06048x - 0.001429\right) \times 100\% \tag{3}$$

The depth–damage function of indoor properties on IL and PBL is

$$f(x) = \left(-0.152x^3 \times 10^{-9} - 0.82x^2 \times 10^{-6} + 1.479x \times 10^{-3} - 0.009\right) \times 100\% \tag{4}$$

The depth–damage function of indoor properties on RL is

$$f(x) = \left(-0.026x^3 \times 10^{-9} - 0.049x^2 \times 10^{-6} + 0.742x \times 10^{-3} - 0.115\right) \times 100\% \tag{5}$$

The depth–damage function of farmland is shown in Table 1. Economic data related to loss assessment are shown in Table 2.

Table 1. Depth–damage function of farmland.

Inundation Depth (m)	[0, 0.5)	[0.5, 1)	[1, 1.5)	[1.5, 2.5)
Damage Ratio (%)	55	70	80	95

Table 2. Explanation of economic data related to loss assessment.

Categories	Price (CNY/m²)	Data Source
Industrial construction costs (A standard factory building cost benchmark)	1100	
Indoor properties of industrial buildings (Output of industrial enterprises above a designated size)	1460	
Construction cost of public buildings (Cost benchmark for ordinary office buildings, shops, and schools)	1500	
Indoor properties of public buildings (Consistent with indoor properties of residential buildings)	800	*Jiading District Statistical Yearbook (2020), Shanghai Statistical Yearbook (2020), Reference Standards for Cost of Various Construction Projects in Shanghai*
Residential construction costs (A commercial housing cost benchmark)	1400	
Indoor properties of residential buildings (Field research)	800	
Farmland properties (Output of the planting industry in 2020)	5.5	

2.3. Methods

　　Firstly, the SCS model and equal-volume method were used for rainstorm waterlogging inundation simulation under precipitation scenarios with return periods of 10, 50, and 100 years. Secondly, the Future Land Use Simulation (FLUS) model was used to simulate the spatial distribution of three land use scenarios in 2040. Thirdly, by overlaying the three precipitation scenarios with the three future land use scenarios, we analyzed the risk exposure elements related to land use. Fourthly, the economic losses under different precipitation and land use scenarios were calculated by combining with the depth–damage functions. (Figure 2). This study aims to analyze the interaction mechanism between different land use patterns and the rainstorm waterlogging disaster risk to enlighten individuals engaged in rainstorm waterlogging disaster risk management and land use management.
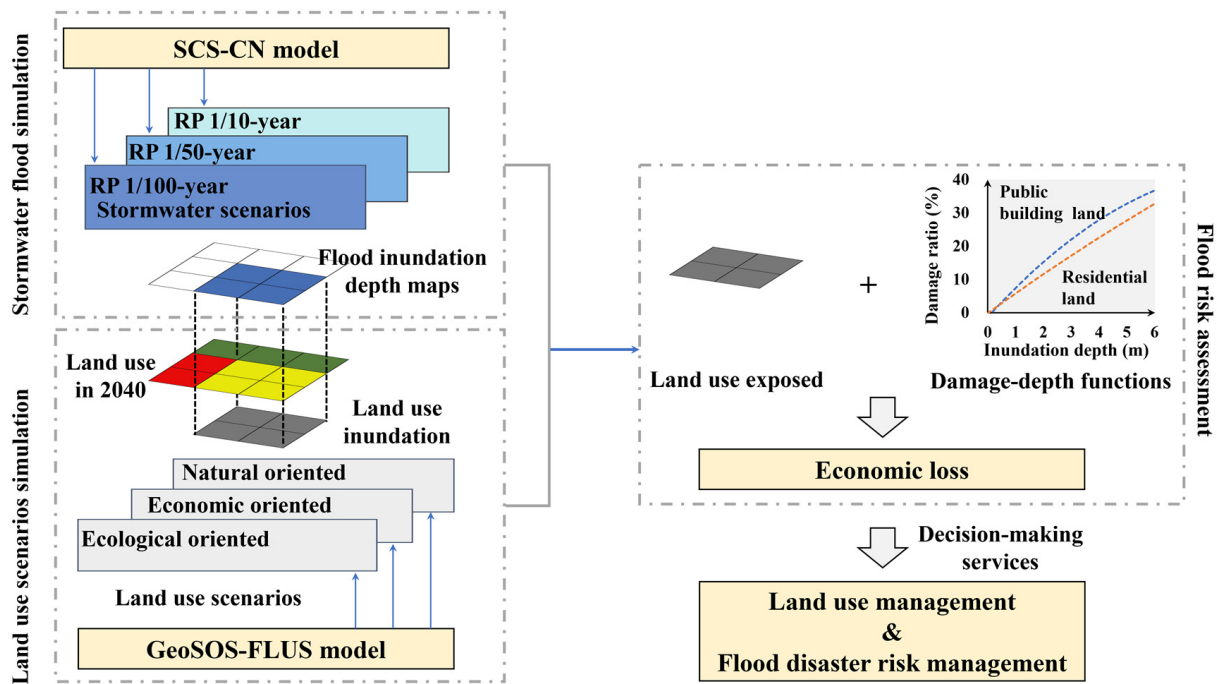

Figure 2. Methodological framework of this study.

2.3.1. GIS-Based Simulation on Rainstorm Waterlogging Disaster

　　(1) SCS Model

　　The SCS model is an empirical hydrological model created by the *U.S. Department of Agriculture's Soil Conservation Service* (USDA-SCS) in the 20th century. It is mainly used for spatial runoff simulation analysis. This model is characterized by its high accuracy, minimal parameters, and easy calculations [51]. It is widely used in various spatial scales [52] and commonly employed in precipitation runoff simulation at different scales in Shanghai [44,50]. The runoff formula of the SCS model is

$$Q = \begin{cases} \frac{(P-Ia)^2}{P+S-Ia}, & P \geq Ia \\ 0, & P < Ia \end{cases} \tag{6}$$

where Q is runoff depth (mm), P is the total precipitation amount for a single precipitation event (mm), Ia is an initial abstraction (mm), and S is the maximum potential retention of the watershed (mm). However, it is difficult to quantify directly the variable Ia, and the variable S exhibits relatively high instability, so the curve number (CN) value is introduced as follows:

$$Ia = 0.2S \tag{7}$$

$$S = \frac{25400}{CN} - 254 \tag{8}$$

where the *CN* value reflects the characteristics of the study area before rainfall, the amount of which ranges from 0 to 100 and is influenced by a combination of factors such as land use type, soil type, and the antecedent moisture conditions (AMC) of the soil. The AMC of the soil are generally divided into three levels: dry (AMCI), normal (AMCII), and wet (AMCIII). In this study, the AMC were set to AMCII based on a combination of the characteristics of Jiangqiao Town and previous research [53]. Finally, the CN value of Jiangqiao Town was determined according to the table of CN value parameters of the SCS model (Table 3). In the SCS model, soil types are categorized based on their infiltration rates into four distinct categories: A, B, C, and D. Type A soils typically consist of deep, well-drained sands or gravels. Type B soils are often sandy loam soils with moderate depth and drainage. Type C soils may have a layer that impedes water movement or be composed of moderately fine to fine texture materials. Type D soils are usually clay soils with high swelling potential, shallow soils over nearly impervious material, or soils with a high water table. The soil types of Jiangqiao Town are classified into three distinct categories (labeled as A, B, and D).

Table 3. Runoff curve numbers of Jiangqiao Town under AMCII.

Land Use	CN Value for Hydrologic Soil Group		
	A	B	D
Green land	34	60	80
Farmland	67	76	86
Water area	100	100	100
Industrial land	89	92	95
Other land	69	80	86
Residential land	77	85	92
Transportation land	98	98	98
Public building land	90	93	96

(2) GIS-based simulation of runoff depth

The runoff depth for each grid can be derived by overlaying the land use map and the soil type map, inputting CN values and precipitation amounts, and applying the appropriate formulas, i.e., (6) to (8). Because Jiangqiao Town is located in the area outside the outer ring road of Shanghai, which is self-draining [50], the drainage facilities are not considered in this study. The total waterlogging volume can be calculated as follows:

$$W = \sum_{i=1}^{n} Q_i \times S_i \qquad (9)$$

where W is the total waterlogging volume of the study area (m^3), Q_i is the runoff depth of the *i*th grid (mm), S_i is the catchment area of the *i* grid (m^2), and *n* is the total number of grids.

In this study, all grids in the DEM of Jiangqiao below the flood elevation height are recorded as inundation areas. Inundation maps of Jiangqiao Town can be created using the equal-volume method in ArcGIS. The equal-volume method is characterized by easy calculations and minimal parameters, which can be used to analyze the range and depth of rainstorm waterlogging disasters [54].

2.3.2. Land Use Simulation Based on GeoSOS-FLUS Model

Based on the land use data for Jiangqiao Town in 2020, and combined with previous studies [55,56] and references to the *Jiangqiao Town Master Plan and Land Use Master Plan (2015–2040)*, three land use scenarios for 2040 (Scenario ND, Scenario EG, and Scenario EP) were simulated by using the GeoSOS-FLUS model (Table 4).

Table 4. The design of land use scenarios for 2040.

Land Use Scenarios	Explanation
Natural development scenario (Scenario ND)	This refers to a situation in which land use change is not significant, there has been no excessive interference from human society, and the study area is in a state of natural development.
Economic growth scenario (Scenario EG)	This refers to the rapid expansion of urban areas while strictly adhering to the constraints of the bottom line of planning, and, in this case, the study area is in a state of rapid urbanization.
Ecological development priority scenario (Scenario EP)	This refers to the continuous expansion of ecological area, aimed at alleviating ecological and environmental problems, and, in this case, the study area is in an ecologically livable state.

In terms of parameters, in the template part of the probabilistic operation, the sampling parameter was set to 10, the number of hidden layers of the neural network was set to 6, and the driving factors include the natural factors (DEM, slope, and water area) as well as the traffic influence factor (roads). In the template part of the cellular automaton (CA), the number of iterations was set to 200, the neighborhood value was set to 3, the acceleration factor was set to 0.4, and the river serves as the restriction conversion area. Finally, the cost matrix was set to three land use scenarios. In addition, the neighborhood weight values of TL, RL, PBL, OL, farmland, IL, WA, and GL were set to 1, 1, 1, 1, 1, 0.7, 1, 0.5, and 0.5, respectively.

2.3.3. Landscape Pattern Analysis

Based on the characteristics of Jiangqiao Town, the landscape pattern analysis of future land use scenarios included the following indices: number of patches (NP), class area (CA), aggregation index (AI), and landscape shape index (LSI) (Table 5).

Table 5. Indices and explanations of landscape patterns.

Landscape Pattern Index	Formula	Explanation
Class area (CA)	$CA = \sum_{j=1}^{n} a_{ij}\left(\frac{1}{10000}\right)$	This refers to the total area of a certain patch type, which is a component of the landscape and also the basis for calculating other indicators.
Number of patches (NP)	$NP = n$	This reflects the spatial pattern of the landscape, which can be used to describe landscape heterogeneity.
Landscape shape index (LSI)	$LSI = \frac{0.25C_{ij}}{\sqrt{a_{ij}}}$	This reflects the degree of aggregation based on the shape characteristics of types of patches.
Aggregation index (AI)	$AI = \frac{g_{ii}}{max g_{ii}}$	This reflects the concentration levels of certain patches.

Note: i is the patch type, a_{ij} is the patch area (m²), C_{ij} is the patch circumference (m), n is the total number of patches, and g_{ii} is the number of adjacent grid units between patch types.

3. Results

3.1. Land Use Change in Jiangqiao Town from 1980 to 2020

From 1980 to 2020, significant changes occurred in the land use structure of Jiangqiao Town, characterized by a notable reduction in farmland and a significant increase in impermeable surfaces (Table 6). In particular, the area of IL increased the most, with a net increase of 11.25 km², while TL and RL also increased by 6.23 km² and 4.59 km²,

respectively. By 2020, the proportion of these three land use types reached 64%. At the same time, there was a net loss of 27.31 km^2 of farmland, constituting a dramatic decrease. In terms of spatial distribution, changes primarily occurred in the western region and sporadically in the southern and northern parts of the study area (Figure 3). It is worth noting that IL currently accounts for the largest proportion and is mostly adjacent to RL.

Table 6. Land use change in Jiangqiao Town from 1980 to 2020 (km^2).

| Land Use	1980	1990	2000	2006	2013	2020	1980 to 2022
Green land	3.56	3.56	0.88	0.88	1.76	4.06	0.50
Farmland	33.55	27.06	23.46	20.24	10.33	6.24	−27.31
Water area	0.27	0.27	2.31	2.24	1.93	2.42	2.15
Industrial land	0.00	5.68	5.42	7.59	10.86	11.25	11.25
Other land	0.00	0.00	0.15	0.65	1.04	2.20	2.20
Residential land	3.64	4.45	7.27	7.34	9.35	8.23	4.59
Transportation land	1.16	1.16	2.67	3.24	6.63	7.39	6.23
Public building land	0.00	0.00	0.10	0.16	0.40	0.48	0.48
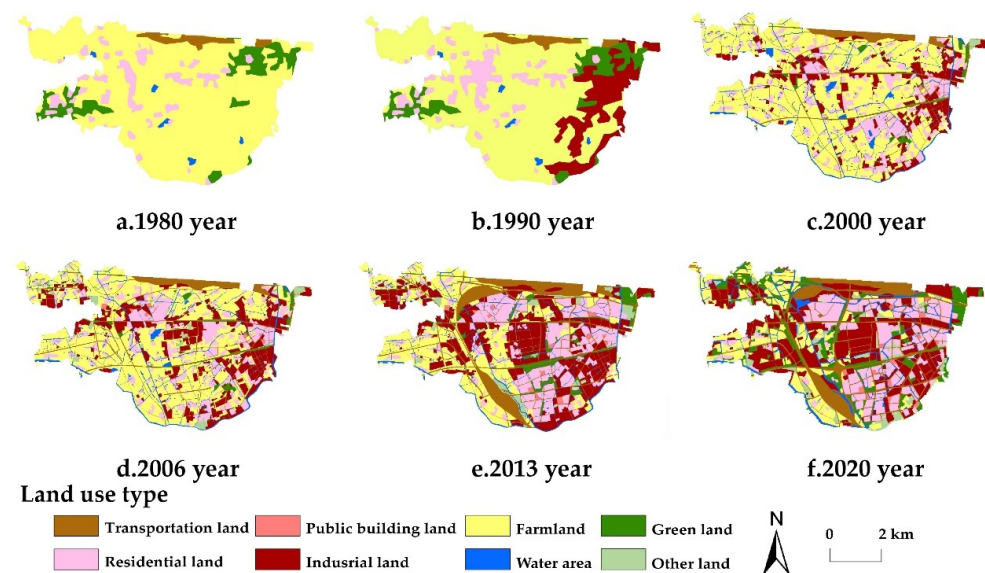
Figure 3. Spatial distribution of Jiangqiao land use from 1980 to 2020.

3.2. Rainstorm Waterlogging Simulation

To obtain the average surface runoff depth for six phases of land use in Jiangqiao Town based on three precipitation scenarios with return periods of 10, 50, and 100 years, the SCS model was run in the GIS environment (Table 7). As depicted in Table 7, under the same land use scenario, the average surface runoff depth is positively correlated with the return period of rainstorms. For instance, considering the average surface runoff depth in 1980 as an example, the precipitation scenario with a 50-year return period exhibited an increase in rainfall by 1.6 cm compared to the precipitation scenario with a 10-year return period, and the precipitation scenario with a 100-year return period exhibited an increase in rainfall by 0.8 cm compared to the precipitation scenario with a 50-year return period. Moreover, under the same precipitation scenario, the average surface runoff depth is positively correlated with urbanization level. For example, in the context of the precipitation scenario with a 10-year return period, the average surface runoff depth was 2.1 cm in 1980, while it was 3.8 cm in 2020.

Table 7. Average surface runoff depth in different rainstorm scenarios (cm).

Year	Return Period		
	10-Year	**50-Year**	**100-Year**
1980	2.1	3.7	4.5
1990	2.4	4.0	4.9
2000	2.9	4.7	5.6
2006	3.1	5.0	5.9
2013	3.7	5.7	6.7
2020	3.8	5.7	6.7

On this basis, further analysis was conducted on the inundation characteristics of land use types under different precipitation scenarios based on the equal-volume method (Figure 4). It can be observed that under the same precipitation scenario, the total waterlogging amount, inundation area, and maximum inundation depth increase year by year with the increase in the urbanization level of Jiangqiao Town. Specially, these characteristics are more significant in comparison to the two stages of 1990 to 2000 and 2006 to 2013. In addition, the inundation depth under the three precipitation scenarios is mainly concentrated in the range of 0 cm to 15 cm. From the perspective of spatial characteristics, the maximum inundation depth occurs in the southern area of Jiangqiao Town, where the terrain is lower and the impermeable surfaces are more concentrated.
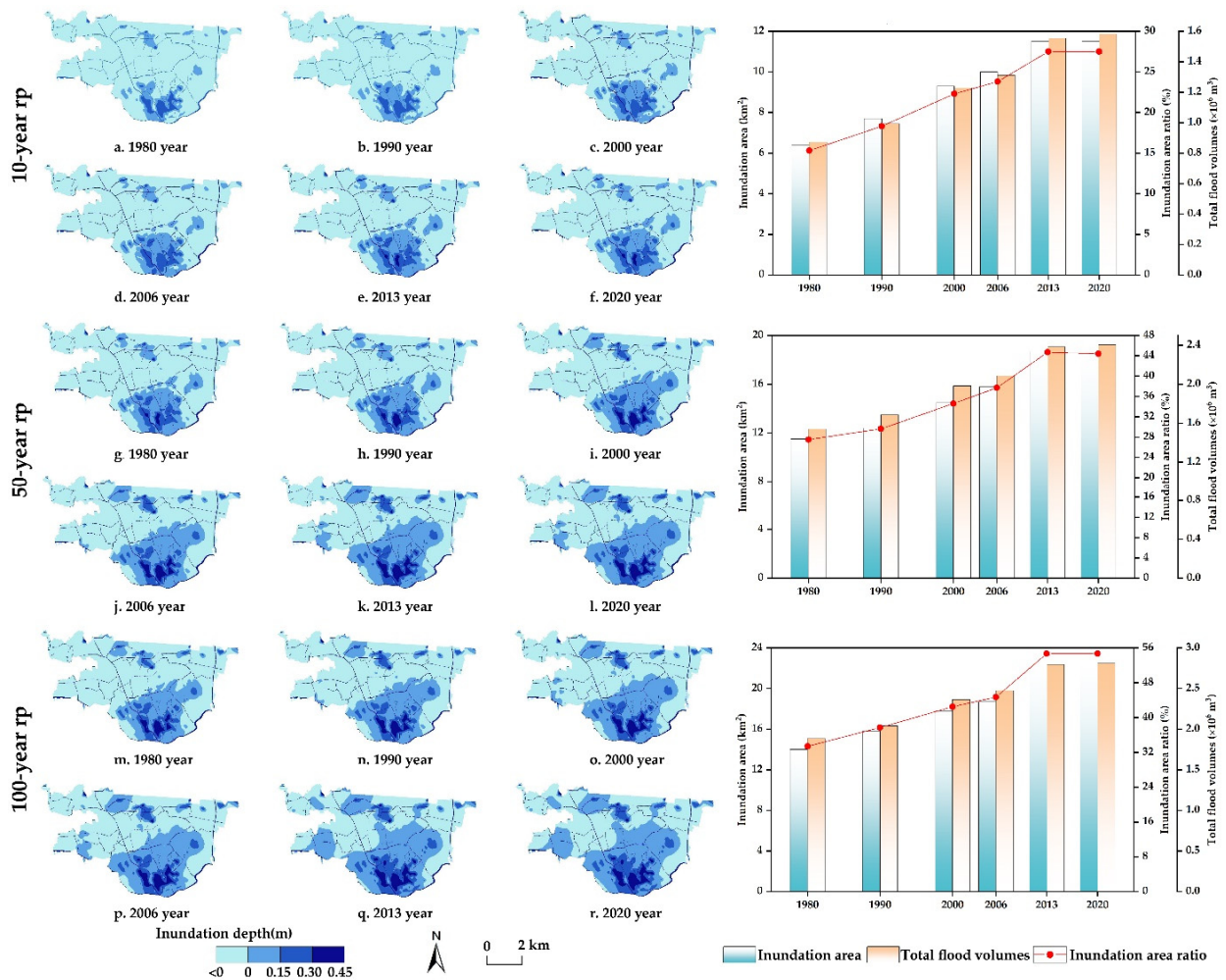

Figure 4. Spatial distribution of inundation depth in different rainstorm scenarios.

3.3. Impact of Land Use Change on Rainstorm Waterlogging

In this section, the precipitation scenario with a 100-year return period was selected. This study analyzed the impact of land use changes on rainstorm waterlogging in the context of rapid urbanization by comparing the surface runoff and inundation depths between two land use scenarios in Jiangqiao Town in 1980 and 2020.

3.3.1. Impact of Land Use Change on Surface Runoff Depth

As shown in Figure 5, in 1980, the surface runoff depths of both TL and RL exceeded 60 mm, with relatively scattered distribution characters, while the runoff depth of farmland was mainly concentrated in the range of 20.2 mm to 40.4 mm. During this period, farmland was the main land use, so there were fewer areas with high runoff depth in Jiangqiao Town as a whole in 1980. As of 2020, the land use of Jiangqiao Town has changed significantly, with a rapid expansion of construction land, including TL, PBL, IL, and RL, and a significant reduction in farmland, resulting in significant changes in surface runoff depth. In 2020, areas of high runoff depth significantly increased, mainly distributed in the eastern, southern, central, northern, and northwestern regions of Jiangqiao Town, similar to the distribution pattern of impermeable surfaces. Meanwhile, areas with low runoff depth have significantly decreased and are distributed in the western, northwestern, and southwestern regions of the study area, which are also relatively concentrated areas of farmland.
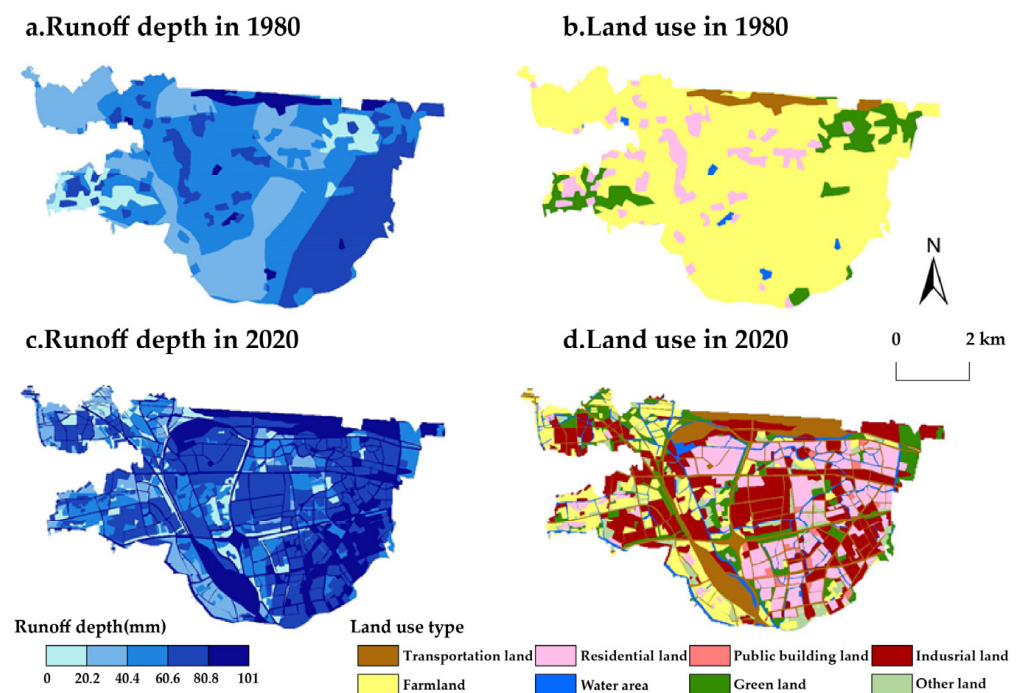

Figure 5. Comparison of surface runoff depth and land use change in 1980 and 2020.

3.3.2. Impact of Land Use Change on Inundation Depth

In this study, four significantly changed land use types (TL, RL, IL, and farmland) were selected to analyze the impact of land use changes on inundation depth (Figure 6). Due to the smaller scale and less significant changes of land use types such as PBL, WA, GL, and OL, they are not discussed here.

On the whole, the expansion of TL, RL, and IL could lead to an increase in inundation depth, while farmland could effectively mitigate the degree of inundation to a certain extent. By comparing Figure 6a,c, it can be found that the increased TL in the southwest region of Jiangqiao Town has led to an increase in inundation depth from 0.36 m to 0.45 m. In 1980, RL was less affected by rainstorm waterlogging. However, after urbanization expanded from north to south, the inundation depth of RL was distributed among all districts in

2020, especially in the southern region, where the inundation depth of some areas of RL has exceeded 0.36 m. In addition, IL has continuously expanded to the northwestern, western, central, and southeastern regions of Jiangqiao Town since 1980, and the above areas are significantly affected by rainstorm waterlogging, especially in the central and southeast regions, with a maximum inundation depth of more than 0.18 m. Meanwhile, the inundation depth of this area was less than 0.09 m in 1980. As for farmland, it was the main land use pattern in Jiangqiao Town in 1980. During this period, flooded areas were concentrated in southern Jiangqiao Town, where the terrain is lower, with an inundation depth of less than 0.09 m. By comparing Figure 6c,d, it can be observed that the scale of farmland in Jiangqiao Town has significantly decreased in the past 40 years. Currently, farmland is mainly distributed in the western, northwestern, and southwestern regions of the study area, where the inundation depth remains less than 0.09 m.
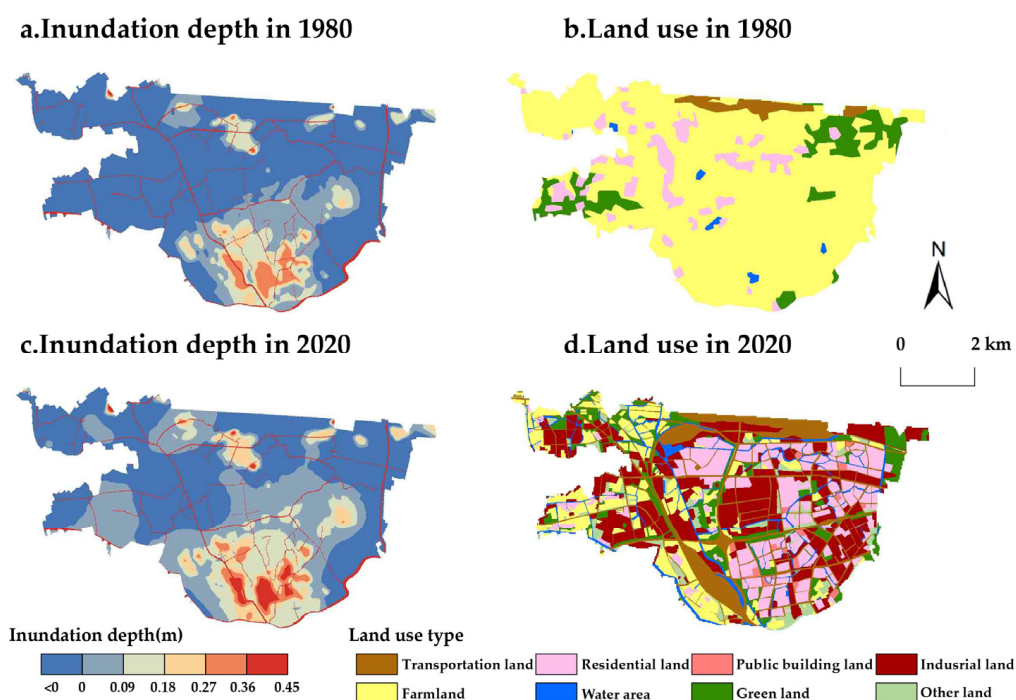
a.Inundation depth in 1980

b.Land use in 1980

c.Inundation depth in 2020

d.Land use in 2020

0 2 km

Inundation depth(m)

<0 0 0.09 0.18 0.27 0.36 0.45

Land use type

 Transportation land Residential land Public building land Indusrial land

 Farmland Water area Green land Other land

Figure 6. Comparison of inundation depth and land use change in 1980 and 2020.

3.4. Rainstorm Waterlogging Disaster Risk Assessment regarding Future Land Use

3.4.1. Land Use Scenario Simulations for 2040

This study took the 2000 and 2020 land use status data for Jiangqiao Town as the initial-year data and the validation data, respectively. Then, the driving factors, including the natural factors as well as the traffic influence factors, were selected to simulate land use in 2020. The simulation results were tested using the actual land uses in 2020 by considering the overall accuracy, the Kappa coefficient, and the Fom index. For the accuracy assessment results, all three accuracy indexes meet the research needs (the overall accuracy is 0.903, the Kappa coefficient is 0.782, and the Fom index is 15.83%). Based on this, the conversion probability was adjusted using different land use scenarios to derive the three land use scenarios in 2040. The spatial distribution of the three land use scenarios in Jiangqiao Town in 2040 is illustrated in Figure 7. It can be found that the three land use scenarios have spatial similarities. This is because the urbanization ratio of Jiangqiao Town reached 99% as early as 2014. Therefore, according to the *Jiangqiao Town Master Plan and Land Use Master Plan (2015–2040)*, all land use types are developed en masse and limited by the master plan. Therefore, to better understand the inherent differences among the three land use scenarios, landscape pattern analysis of the three future land use scenarios was conducted using the landscape pattern index introduced in this study.
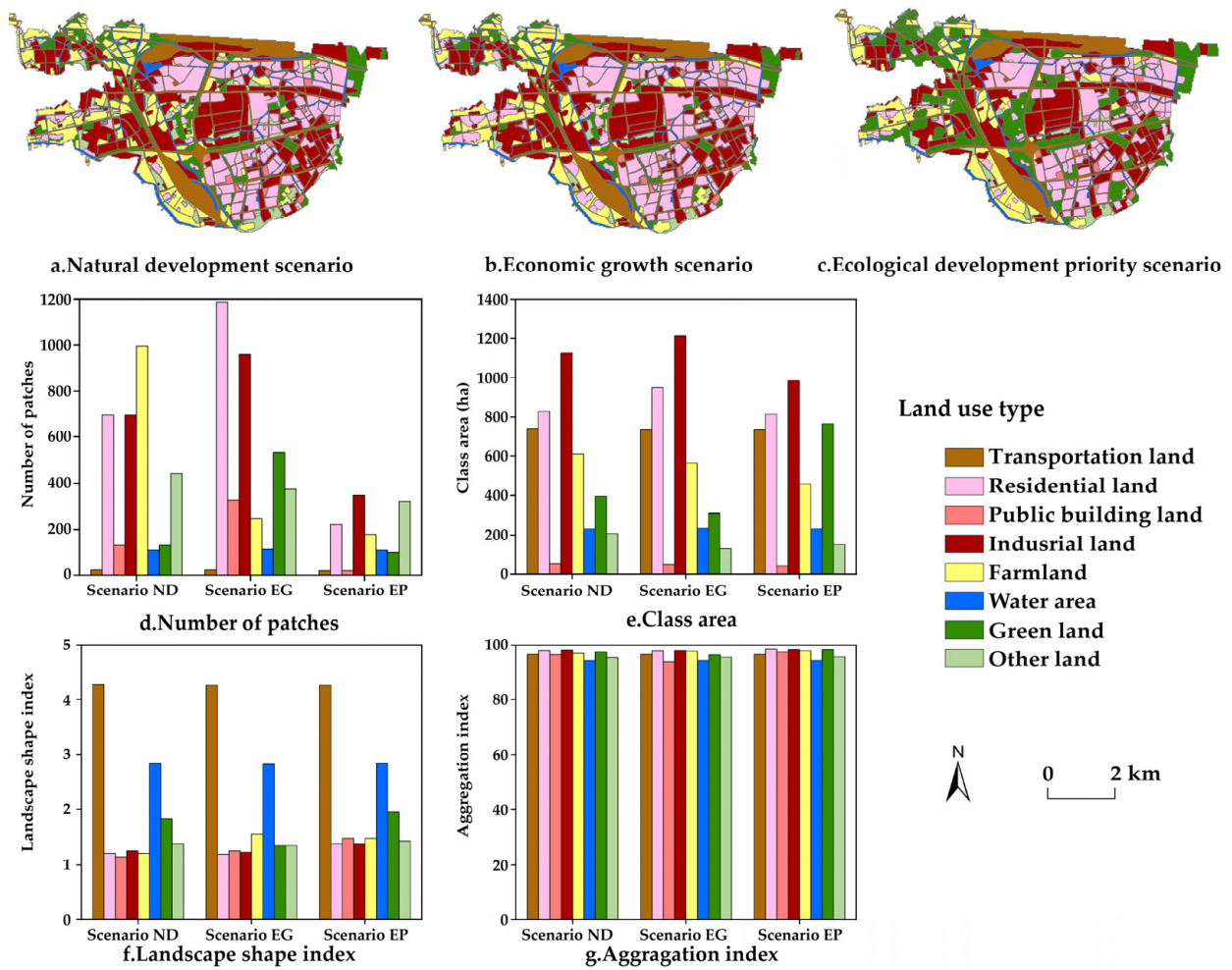
Figure 7. Spatial distribution of land use and landscape pattern in 2040.

As illustrated in Figure 7, at the landscape scale, Scenario EG exhibits the highest degree of land use fragmentation, while Scenario EP shows the lowest fragmentation. The number of patches in Scenario ND is 3239, that in Scenario EG is 3768, and that in Scenario EP is 1337. At the patch-type scale, under Scenario ND and Scenario EG, RL, IL, and farmland patches dominate in terms of both area and quantity. Under Scenario EP, GL, RL, and IL patches dominate in terms of both area and quantity. It can be observed that the LSI and AI show similarities across the three land use scenarios, while there are significant differences in NP and CA.

3.4.2. Rainstorm Waterlogging Simulation in Different Land Use Scenarios

To further explore rainstorm waterlogging inundation under different land use scenarios, we generated rainstorm waterlogging inundation maps for three future land use scenarios under the precipitation scenarios with return periods of 10, 50, and 100 years based on the SCS model and the equal-volume method. These maps are presented in Figure 8.

As shown in Figure 8, due to the relatively large area of GL and farmland, lesser extent of built-up area, and well-planned land use spatial layout in Scenario EP, the mitigation effect of rainstorm waterlogging risk is greater compared to such effects in Scenario ND and Scenario EG under the same precipitation scenario. For example, under the precipitation scenario with a 100-year return period, only the inundation area in Scenario EP is less than 50% of the study area, while in Scenario ND and Scenario EG, the inundation areas are both greater than 50% of Jiangqiao Town. In addition, as the return period of precipitation scenarios increases, the rainstorm waterlogging disaster risk mitigation effect of land use in Scenario EP gradually becomes less significant but remains better than that for Scenario

ND and Scenario EG. Meanwhile, the inundation area in Scenario EP is consistently the smallest across all three precipitation scenarios. However, with the increase in the return period of precipitation events, the change in inundation area in Scenario EP compared to Scenario ND and Scenario EG shows a growing trend but with a gradually decreasing rate of increase. For instance, under precipitation scenarios with return periods of 10, 50, and 100 years, the inundation area in Scenario EP decreased by 0.5 km^2, 1.2 km^2, and 1.2 km^2, respectively, compared to Scenario ND. Compared to Scenario EG, the inundation area in Scenario EP decreased by approximately 0.9 km^2, 1.8 km^2, and 1.9 km^2, respectively.

a.Scenario ND with 10-year rp   **b.Scenario ND with 50-year rp**   **c.Scenario ND with 100-year rp**

d.Scenario EG with 10-year rp   **e.Scenario EG with 50-year rp**   **f.Scenario EG with 100-year rp**

g.Scenario EP with 10-year rp   **h.Scenario EP with 50-year rp**   **i.Scenario EP with 100-year rp**

Inundation depth(m)
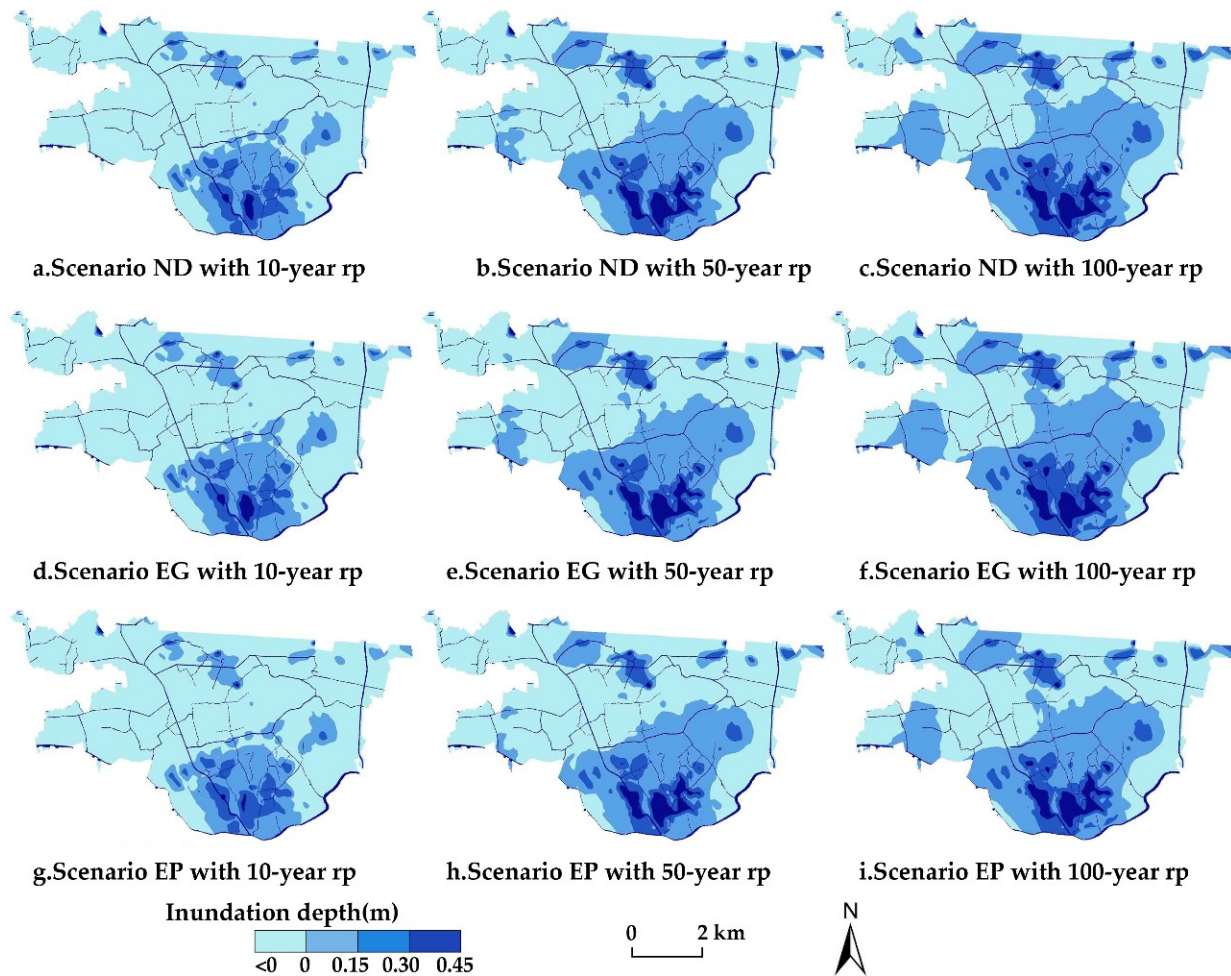<0   0   0.15   0.30   0.45

0   2 km

N

Figure 8. Spatial distribution of inundation area in different land use scenarios.

3.4.3. Rainstorm Waterlogging Disaster Risk Assessment in Different Land Use Scenarios

To further explore the relationship between different land use scenarios and losses from rainstorm waterlogging disasters, spatial distribution maps of inundation losses in different land use scenarios in Jiangqiao Town were generated (Figure 9) based on Formulas (2)–(5) and related economic data.

As depicted in Figure 9, under precipitation scenarios with return periods of 10, 50, and 100 years, the total economic losses in Scenario ND are CNY 560 million, CNY 890 million, and CNY 1.07 billion, respectively. In Scenario EG, the total economic losses are CNY 630 million, CNY 980 million, and CNY 1.19 billion, respectively. In Scenario EP, the total economic losses are CNY 480 million, CNY 750 million, and CNY 910 million, respectively. The total economic loss in Scenario EP is the lowest under the same precipitation scenario. In addition, the total loss in Scenario EP under the precipitation scenario with a 100-year return period is CNY 910 million, which is even lower than the total loss in Scenario EG under the precipitation scenario with a 50-year return period. These findings highlight

that land use under Scenario EP significantly reduces the rainstorm waterlogging losses compared to those in Scenario ND and Scenario EG.
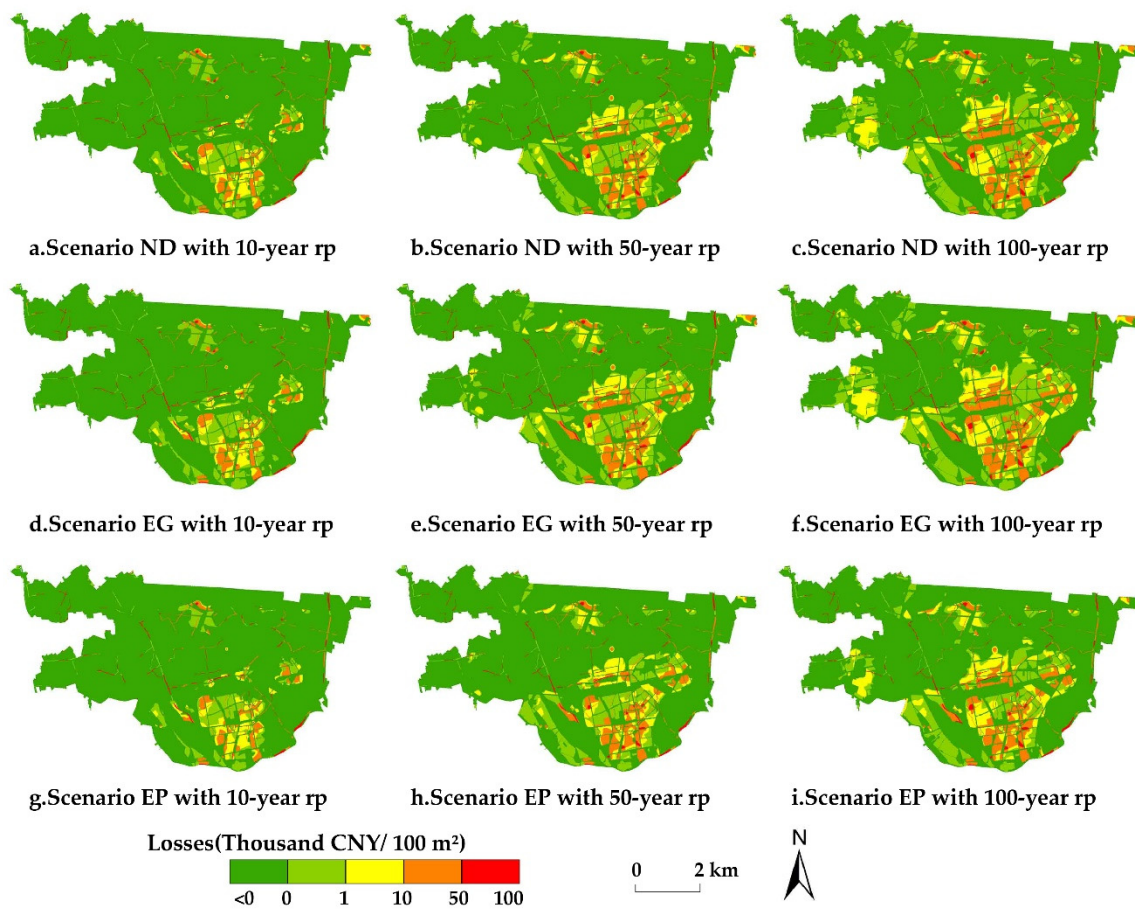

Figure 9. Spatial distribution of inundation losses in different land use scenarios.

4. Conclusions

Based on the scenario analysis method, the rainstorm waterlogging disaster risk was analyzed in multiple interactional scenarios of rainstorm events in and land use pattern models of Jiangqiao Town. The main findings are as follows.

Precipitation intensity is a significant factor influencing the risk of rainstorm waterlogging disaster. Under the same land use pattern, the increase in precipitation intensity will exacerbate the risk of urban rainstorm waterlogging disasters, which is consistent with existing research [57]. From the precipitation scenario with the return period ranging from 10 to 100 years, the total losses of Scenario ND are CNY 560 million, CNY 890 million, and CNY 1.07 billion, respectively, and those of Scenario EG are CNY 630 million, CNY 980 million, and CNY 1.19 billion, respectively, while those of Scenario EP are (in order) CNY 480 million, CNY 750 million, and CNY 910 million.

Different land use patterns exhibit varying mitigation effects on urban rainstorm waterlogging disaster risk. The increase in impermeable surfaces, such as residential land, and the decrease in farmland driven by urbanization have resulted in an annual increase in surface runoff, inundation area, and inundation depth in Jiangqiao Town. Previous studies have demonstrated that under the same level of rainstorm hazard, the areas of medium- and high-risk patches exhibit an obvious increasing trend with the expansion of construction land [58]. This finding is consistent with the results of this study. Under the same precipitation intensity, the total losses in land use scenario EP are the lowest compared to those in land use scenarios ND and EG, which are much more pronounced under precipitation scenarios with return periods of 10 years and 50 years.

The ecological development prioritization land use pattern significantly mitigates the risk of rainstorm waterlogging disaster, which provides a theoretical foundation for the use of ecological measures in flood control. Based on the results of the analysis, it can be conducted that, given a fixed urban scale, increasing ecological spaces and regulating the expansion of construction land can significantly reduce the risk of urban rainstorm waterlogging disasters. Specific measures, such as the implementation of concave green spaces [59] and the development of rain gardens [60], should be considered.

This study also found that the land use pattern under Scenario EP exhibits limited effectiveness in mitigating waterlogging risk under the precipitation scenario with the 100-year return period. This study confirms that changing land use patterns can mitigate rainstorm waterlogging disaster risk by altering the exposure states of various land use types to such risk. However, disaster risk is jointly affected by hazards, exposure, and vulnerability [61]. It is important to note that this approach represents only one aspect of broader waterlogging disaster risk management, and additional measures may be necessary to address the full spectrum of risks, especially under extreme weather conditions. It is essential to integrate grey infrastructure, green infrastructure, and institutional policies into land use management decision-making processes [62,63]. It is important to acknowledge that with urban construction and development, the drainage infrastructure in Jiangqiao Town has gradually improved, yet the characteristics of self-drainage remain distinctly evident because the town is located outside the outer ring road of Shanghai. In addition, the existing drainage network for Jiangqiao Town is classified as confidential, which results in a lack of available drainage data and means that drainage effects are not considered in this study. To better enhance Jiangqiao's adaptability to rainstorm waterlogging disaster risk, future research should combine land use changes with drainage facility improvements.

This study aims to analyze the interaction mechanism between different land use patterns and the rainstorm waterlogging disaster risk, providing insights for rainstorm waterlogging disaster risk management. However, it is necessary to further elucidate risk thresholds to determine when land use strategies begin to significantly reduce flood risk, especially in the context of specific projects. Building on this, more practical and feasible recommendations can be developed for land use management decision making. In addition, due to the use of a unified cost benchmark for building costs, it is challenging to estimate the indoor characteristics of industrial and public buildings. As a result, the indoor characteristics of buildings have been used as substitutes. To improve the accuracy of loss assessments, future research should aim to refine the economic data related to loss assessment to ensure that evaluations are more reflective of actual conditions.

Author Contributions: H.X. conceived the research's framework, developed research objectives, and revised the manuscript; J.G. conducted the data analysis and wrote, translated, and revised the manuscript; X.Y. collected the data and wrote the manuscript; Q.Q. revised the manuscript and edited and refined its English. S.D. and J.W. made suggestions for revising and improving the research. All authors have read and agreed to the published version of the manuscript.

Data Availability Statement: Data sharing is not applicable to this article.

Conflicts of Interest: The authors declare no conflict of interest.

References

1. Myhre, G.; Alterskjær, K.; Stjern, C.W.; Hodnebrog, Ø.; Marelle, L.; Samset, B.H.; Sillmann, J.; Schaller, N.; Fischer, E.; Schulz, M.; et al. Frequency of extreme precipitation increases extensively with event rareness under global warming. *Sci. Rep.* **2019**, *9*, 16063. [CrossRef] [PubMed]
2. Field, C.B.; Barros, V.; Stocker, T.F.; Dahe, Q. *Managing the Risks of Extreme Events and Disasters to Advance Climate Change Adaptation: Special Report of the Intergovernmental Panel on Climate Change*, 1st ed.; Cambridge University Press: Cambridge, UK, 2012.

3. CRED. 2022 Disaster in Numbers [DS/OL]. 2023. Available online: https://cred.be/sites/default/files/2022_EMDAT_report.pdf (accessed on 3 January 2024).

4. Gashaw, T.; Tulu, T.; Argaw, M.; Worqlul, A.W. Modeling the hydrological impacts of land use/land cover changes in the Andassa watershed, Blue Nile Basin, Ethiopia. *Sci. Total Environ.* **2018**, *619–620*, 1394–1408. [CrossRef] [PubMed]

5. Woldemichael, A.T.; Hossain, F.; Pielke, R., Sr. Evaluation of surface properties and atmospheric disturbances caused by post-dam alterations of land use/land cover. *Hydrol. Earth Syst. Sci.* **2014**, *18*, 3711–3732. [CrossRef]

6. Hounkpè, J.; Diekkrüger, B.; Afouda, A.A.; Sintondji, L.O. Land use change increases flood hazard: A multi-modelling approach to assess change in flood characteristics driven by socio-economic land use change scenarios. *Nat. Hazards* **2019**, *98*, 1021–1050. [CrossRef]

7. Janizadeh, S.; Chandra Pal, S.; Saha, A.; Chowdhuri, I.; Ahmadi, K.; Mirzaei, S.; Mosavi, A.H.; Tiefenbacher, J.P. Mapping the spatial and temporal variability of flood hazard affected by climate and land-use changes in the future. *J. Environ. Manag.* **2021**, *298*, 113551. [CrossRef] [PubMed]

8. Yang, X.; Ren, L.; Singh, V.P.; Liu, X.; Yuan, F.; Jiang, S.; Yong, B. Impacts of land use and land cover changes on evapotranspiration and runoff at Shalamulun River watershed, China. *Hydrol. Res.* **2012**, *43*, 23–37. [CrossRef]

9. Huong HT, L.; Pathirana, A. Urbanization and climate change impacts on future urban flooding in Can Tho city, Vietnam. *Hydrol. Earth Syst. Sci.* **2013**, *17*, 379–394. [CrossRef]

10. Tang, J.; Li, Y.; Cui, S.; Xu, L.; Hu, Y.; Ding, S.; Nitivattananon, V. Analyzing the spatiotemporal dynamics of flood risk and its driving factors in a coastal watershed of southeastern China. *Ecol. Indic.* **2021**, *121*, 107134. [CrossRef]

11. Muis, S.; Güneralp, B.; Jongman, B.; Aerts, J.C.J.H.; Ward, P.J. Flood risk and adaptation strategies under climate change and urban expansion: A probabilistic analysis using global data. *Sci. Total Environ.* **2015**, *538*, 445–457. [CrossRef]

12. Rahmati, O.; Darabi, H.; Panahi, M.; Kalantari, Z.; Naghibi, S.A.; Ferreira, C.S.S.; Kornejady, A.; Karimidastenaei, Z.; Mohammadi, F.; Stefanidis, S.; et al. Development of novel hybridized models for urban flood susceptibility mapping. *Sci. Rep.* **2020**, *10*, 12937. [CrossRef]

13. Nicholls, R.J.; Reeder, T.; Brown, S.; Haigh, I.D. *The Risks of Sea-Level Rise for Coastal Cities*; Centre of Science and Policy: Cambridge, UK, 2017.

14. Ke, Q.; Jonkman, S.; Van Gelder, P.; Bricker, J.D. Frequency Analysis of Storm-Surge-Induced Flooding for the Huangpu River in Shanghai, China. *J. Mar. Sci. Eng.* **2018**, *6*, 70. [CrossRef]

15. Shan, X.; Wen, J.; Zhang, M.; Wang, L.; Ke, Q.; Li, W.; Du, S.; Shi, Y.; Chen, K.; Liao, B.; et al. Scenario-Based Extreme Flood Risk of Residential Buildings and Household Properties in Shanghai. *Sustainability* **2019**, *11*, 3202. [CrossRef]

16. Tsakiris, G. Flood risk assessment: Concepts, modelling, applications. *Nat. Hazards Earth Syst. Sci.* **2014**, *14*, 1361–1369. [CrossRef]

17. Winsemius, H.C.; Van Beek LP, H.; Jongman, B.; Ward, P.J.; Bouwman, A. A framework for global river flood risk assessments. *Hydrol. Earth Syst. Sci.* **2013**, *17*, 1871–1892. [CrossRef]

18. Ganguli, P.; Reddy, M.J. Probabilistic assessment of flood risks using trivariate copulas. *Theor. Appl. Climatol.* **2013**, *111*, 341–360. [CrossRef]

19. Wang, Y.; Liu, M.; Xing, Z.; Liu, H.; Song, J.; Hou, Q.; Xu, Y. Study of Nonstationary Flood Frequency Analysis in Songhua River Basin. *Water* **2023**, *15*, 3443. [CrossRef]

20. Chen, W.; Huang, G.; Zhang, H. Urban stormwater inundation simulation based on SWMM and diffusive overland-flow model. *Water Sci. Technol.* **2017**, *76*, 3392–3403. [CrossRef] [PubMed]

21. Maryam, M.; Kumar, R.; Thahaby, N. Assessment of the Hydraulic Performance of the Urban Drainage System due to Climate Change using DHI MIKE URBAN. *J. Biomed. Res. Environ. Sci.* **2021**, *2*, 261–267. [CrossRef]

22. Verma, R.K.; Verma, S.; Mishra, S.K.; Pandey, A. SCS-CN-Based Improved Models for Direct Surface Runoff Estimation from Large Rainfall Events. *Water Resour. Manag.* **2021**, *35*, 2149–2175. [CrossRef]

23. Sharma, S.; Roy, P.S.; Chakravarthi, V.; Srinivasarao, G.; Bhanumurthy, V. Extraction of detailed level flood hazard zones using multi-temporal historical satellite data-sets—A case study of Kopili River Basin, Assam, India. *Geomat. Nat. Hazards Risk* **2017**, *8*, 792–802.

24. Chawan, A.; Kakade, V.; Jadhav, J. Automatic Detection of Flood Using Remote Sensing Images. *J. Inf. Technol. Digit. World* **2020**, *02*, 11–26. [CrossRef]

25. Smith, A.; Bates, P.D.; Wing, O.; Sampson, C.; Quinn, N.; Neal, J. New estimates of flood exposure in developing countries using high-resolution population data. *Nat. Commun.* **2019**, *10*, 1814. [CrossRef] [PubMed]

26. Pham, Q.B.; Ali, S.A.; Bielecka, E.; Calka, B.; Orych, A.; Parvin, F.; Łupikasza, E. Flood vulnerability and buildings' flood exposure assessment in a densely urbanised city: Comparative analysis of three scenarios using a neural network approach. *Nat. Hazards* **2022**, *113*, 1043–1081. [CrossRef]

27. Zhang, M.; Zhai, G.; He, T.; Wu, C. A growing global threat: Long-term trends show cropland exposure to flooding on the rise. *Sci. Total Environ.* **2023**, *899*, 165675. [CrossRef] [PubMed]

28. Shrestha, B.B.; Kawasaki, A.; Zin, W.W. Development of flood damage assessment method for residential areas considering various house types for Bago Region of Myanmar. *Int. J. Disaster Risk Reduct.* **2021**, *66*, 102602. [CrossRef]

29. Mobini, S.; Nilsson, E.; Persson, A.; Becker, P.; Larsson, R. Analysis of pluvial flood damage costs in residential buildings—A case study in Malmö. *Int. J. Disaster Risk Reduct.* **2021**, *62*, 102407. [CrossRef]

30. Dong, B.; Xia, J.; Li, Q.; Zhou, M. Risk assessment for people and vehicles in an extreme urban flood: Case study of the "7.20" flood event in Zhengzhou, China. *Int. J. Disaster Risk Reduct.* **2022**, *80*, 103205. [CrossRef]

31. Nithila, A.N.; Shome, P.; Islam, I. Waterlogging induced loss and damage assessment of urban households in the monsoon period: A case study of Dhaka, Bangladesh. *Nat. Hazards* **2022**, *110*, 1565–1597. [CrossRef]

32. Xiao, S.; Zou, L.; Xia, J.; Dong, Y.; Yang, Z.; Yao, T. Assessment of the urban waterlogging resilience and identification of its driving factors: A case study of Wuhan City, China. *Sci. Total Environ.* **2023**, *866*, 161321. [CrossRef]

33. De Moel, H.; Jongman, B.; Kreibich, H.; Merz, B.; Penning-Rowsell, E.; Ward, P.J. Flood risk assessments at different spatial scales. *Mitig. Adapt. Strateg. Glob. Change* **2015**, *20*, 865–890. [CrossRef]

34. De Kok, J.L.; Grossmann, M. Large-scale assessment of flood risk and the effects of mitigation measures along the Elbe River. *Nat. Hazards* **2010**, *52*, 143–166. [CrossRef]

35. Gabriels, K.; Willems, P.; Van Orshoven, J. A comparative flood damage and risk impact assessment of land use changes. *Nat. Hazards Earth Syst. Sci.* **2022**, *22*, 395–410. [CrossRef]

36. Dwarakish, G.S.; Ganasri, B.P. Impact of land use change on hydrological systems: A review of current modeling approaches. *Cogent Geosci.* **2015**, *1*, 1115691. [CrossRef]

37. Patil, N.S.; Nataraja, M. Effect of land use land cover changes on runoff using hydrological model: A case study in Hiranyakeshi watershed. *Model. Earth Syst. Environ.* **2020**, *6*, 2345–2357. [CrossRef]

38. Estrella, M.; Saalismaa, N.; Renaud, F.G. Reduction (Eco-DRR):an overview. In *The Role of Ecosystems in Disaster Risk Reduction*; United Nations University Press: Tokyo, Japan, 2013; Volume 26.

39. Sun, X.; Li, R.; Shan, X.; Xu, H.; Wang, J. Assessment of climate change impacts and urban flood management schemes in central Shanghai. *Int. J. Disaster Risk Reduct.* **2021**, *65*, 102563. [CrossRef]

40. Tu, J.; Wen, J.; Yang, L.E.; Reimuth, A.; Young, S.S.; Zhang, M.; Wang, L.; Garschagen, M. Assessment of building damage and risk under extreme flood scenarios in Shanghai. *Nat. Hazards Earth Syst. Sci.* **2023**, *23*, 3247–3260. [CrossRef]

41. Balica, S.F.; Wright, N.G.; Van Der Meulen, F. A flood vulnerability index for coastal cities and its use in assessing climate change impacts. *Nat. Hazards* **2012**, *64*, 73–105. [CrossRef]

42. Shan, X.; Yin, J.; Wang, J. Risk assessment of shanghai extreme flooding under the land use change scenario. *Nat. Hazards* **2022**, *110*, 1039–1060. [CrossRef]

43. Quan, R. Risk assessment of flood disaster in Shanghai based on spatial–temporal characteristics analysis from 251 to 2000. *Environ. Earth Sci.* **2014**, *72*, 4627–4638. [CrossRef]

44. Quan, R.; Liu, M.; Lu, M.; Zhang, L.; Wang, J.; Xu, S. Waterlogging risk assessment based on land use/cover change: A case study in Pudong New Area, Shanghai. *Environ. Earth Sci.* **2010**, *61*, 1113–1121. [CrossRef]

45. Yin, Z.; Yin, J.; Xu, S.; Wen, J. Community-based scenario modelling and disaster risk assessment of urban rainstorm waterlogging. *J. Geogr. Sci.* **2011**, *21*, 274–284. [CrossRef]

46. Wang, L.; Zhang, M.; Wen, J.; Chong, Z.; Ye, Q.; Ke, Q. Simulation of Extreme compound Costal Flooding in Shanghai. *Adv. Water Sci.* **2019**, *30*, 546–555.

47. *DB31/T 1043–2017*; Standard of Rainstorm Intensity Formula and Design Rainstorm Distribution. Shanghai Engineering Design Institute: Shanghai, China, 2017.

48. Ke, Q. Flood Risk Analysis for Metropolitan Areas: A Case Study for Shanghai. Ph.D. Thesis, TU Delft: Dlft University of Technology, Delft, The Netherlands, 2014.

49. Quan, R. Vulnerability analysis of rainstorm waterlogging on buildings in central urban area of Shanghai based on scenario simulation. *Sci. Geogr. Sin.* **2014**, *34*, 1399–1403.

50. Yin, Z.; Bao, L.; Yin, J. GIS-based study on vulnerability to rainstorm inundation in Pudong of Shanghai. *J. Nat. Disasters* **2011**, *20*, 29–35.

51. Boughton, W.C. A review of the USDA SCS curve number method. *Soil Res.* **1989**, *27*, 511–523. [CrossRef]

52. Yao, L.; Chen, L.; Wei, W.; Sun, R. Potential reduction in urban runoff by green spaces in Beijing: A scenario analysis. *Urban For. Urban Green.* **2015**, *14*, 300–308. [CrossRef]

53. Quan, R.; Liu, M.; Hou, L.; Lu, M.; Zhang, L.; Ou, D.; Xu, S.; Yu, L. Impact of land use dynamic change on surface runoff: A case study on Shanghai Pudong New District. *J. Catastr.* **2009**, *24*, 44–49.

54. Yin, Z.; Xu, S.; Yin, J.; Wang, J. Small-scale based scenario modeling and disaster risk assessment of urban rainstorm water-logging. *Acta Geogr. Sin.* **2010**, *65*, 553–562.

55. Li, W.; Lan, Z.; Chen, D.; Zheng, Z. Multi-scenario simulation of land use and its spatial-temporal response to ecological risk in Guangzhou city. *Bull. Soil Water Conserv.* **2020**, *40*, 204–210.

56. Ma, X.; Lin, P.; Chen, Z. Simulation of Land Use Spatial Layout Based on FLUS Model: A Case Study of Huadu District, Guangzhou. *Adv. Soc. Sci.* **2019**, *8*, 1327–1341.

57. Phinyoyang, A.; Ongsomwang, S. Optimizing Land Use and Land Cover Allocation for Flood Mitigation Using Land Use Change and Hydrological Models with Goal Programming, Chaiyaphum, Thailand. *Land* **2021**, *10*, 1317. [CrossRef]

58. Peng, J.; Wei, H.; Wu, W.H.; Liu, Y.X.; Wang, Y.L. Storm flood disaster risk assessment in urban area based on the simulation of land use scenarios: A case of Maozhou Watershed in Shenzhen City. *Acta Ecol. Sin.* **2018**, *38*, 3741–3755.

59. Du, S.; Wang, C.; Shen, J.; Wen, J.; Gao, J.; Wu, J.; Lin, W.; Xu, H. Mapping the capacity of concave green land in mitigating urban pluvial floods and its beneficiaries. *Sustain. Cities Soc.* **2019**, *44*, 774–782. [CrossRef]

60. Kasprzyk, M.; Szpakowski, W.; Poznańska, E.; Boogaard, F.C.; Bobkowska, K.; Gajewska, M. Technical solutions and benefits of introducing rain gardens—Gdańsk case study. *Sci. Total Environ.* **2022**, *835*, 155487. [CrossRef] [PubMed]
61. Crichton, D. The risk triangle. *Nat. Disaster Manag.* **1999**, *102*, 102–103.
62. Xu, H.; Gao, J.; Yu, X.; Wang, C.; Liu, Y.; Wen, J.; Qin, Q. Study on Suburban Land Use Optimization from the Perspective of Flood Mitigation—A Case Study of Pujiang Country Park in Shanghai. *Sustainability* **2024**, *16*, 3436. [CrossRef]
63. Du, S.; Scussolini, P.; Ward, P.J.; Zhang, M.; Wen, J.; Wang, L.; Koks, E.; Diaz-Loaiza, A.; Gao, J.; Ke, Q.; et al. Hard or soft flood adaptation? Advantages of a hybrid strategy for Shanghai. *Glob. Environ. Chang.* **2020**, *61*, 102037. [CrossRef]